

A Survey of Performance of Fluidic Thrust Vectoring Mechanisms by Numerical and Experimental Studies

Li Li^a, Tsutomu Saito^b

^aSchool of Mechanical Engineering, Dalian Jiaotong University, Dalian, China

^bDepartment of Aerospace Engineering, Muroran Institute of Technology, Muroran, Japan

Abstract

The objectives of this paper are to compare the effect of fluidic thrust vectoring (FTV) parameters on two converging-diverging nozzle models and discuss the relation of evaluation methods between thrust pitching angle and thrust pitching moment. The interaction of a secondary jet with the primary jet flow in two nozzle models is also investigated. Numerical and experimental studies of FTV were done with nozzle model 1 and nozzle model 2. The experiments are carried out with a nozzle pressure ratio (NPR) of 3-10, a secondary pressure ratio (SPR) of 1, 2 and 3, and two different secondary jet locations. Numerical simulations of the nozzle flow are performed with solving the Navier-Stokes equation, and the parameters are the same with the experimental conditions. Combinations of NPR, SPR, and secondary jet location are set to compare the performance of the two nozzle models. The thrust pitching moment and the thrust pitching angle are determined to evaluate the FTV performance. Positive inter-relation between the thrust pitching moment and the thrust pitching angle is found.

1. INTRODUCTION

Thrust vectoring of aircraft is emerging as an important and desirable technology since 1960's. Thrust vectoring technology, an ability of air vehicles to manipulate the nozzle flow to deflect their longitudinal axis, can increase aircraft performance [1-2]. The thrust vectoring (TV) technology provides a host of benefits to the modern air vehicles, such as low cost, light weight, short take-off and landing, as well as radar signature reduction and low sonic-boom signature. Thrust vectoring is prevalent in aircraft as its benefits become more useful and efficient [3-5].

There are two methods to achieve thrust vectoring: mechanical thrust vectoring (MTV) and fluidic thrust vectoring (FTV). MTV nozzles require operated hardware to direct the exhaust flow off nozzle longitudinal axis. Although MTV technologies have been employed in many recent aircrafts, there are some significant disadvantages, such as complexity, weight, high-cost etc. [6-7]. Due to the disadvantage of MTV, researchers want to investigate novel methods to achieve the same thrust vectoring capabilities with simpler mechanisms. Instead of making mechanical parts to create vectored thrust, FTV nozzles use a secondary jet air to manipulate the nozzle main jet flow. It has numerous desirable advantages beyond MTV, such as lightweight, low noise, simplicity, inexpensive maintenance costs, etc. [8-10]. Due to the advantages over conventional means of thrust vectoring, FTV technology is a more suitable nozzle candidate for high-performance aircraft operations and enhance aerospace power [11-13].

In this study, the secondary jet injection is on the wall of the diverging part of the nozzle. The interaction of the secondary flow and the main flow forms an oblique shock wave which makes the main flow deflected as it passes through the oblique shock [14-16].

The nozzle model 1 and model 2 are discussed in the paper. The nozzles are a converging-diverging type with a rectangular cross section. The Mach numbers at the nozzle exit of model 1 and 2 are designed to be 1.5 and 2, respectively. The secondary fluidic injection for thrust vectoring is on the nozzle upper diverging wall. Variations were done on the primary and secondary jet conditions. The study is conducted to evaluate the performance of two nozzle models with thrust pitching moment and

thrust pitching angle, and investigate the effects of parameters and interaction of the secondary injection with the primary flow in two nozzle models for fluidic thrust vectoring.

For the nozzle model 1, it has been found difficult to evaluate the FTV performance quantitatively on the basis of the appearance of downstream flow patterns. So the nozzle model 2 is developed for further study. As expected, if the secondary jet slot is on the nozzle upper wall, the injected flow forms an oblique wave which makes the primary flow turn downwards from the longitudinal axis when the primary flow interacts with the oblique wave.

The thrust pitching moment obtained by force-moment balance and the common thrust pitching angle evaluated from the ratio of the radial to the axial momentums of exhaust gas are discussed.

The relation between the thrust pitching moment and the thrust pitching angle shows the positive inter-relation. Therefore, FTV performance can be evaluated with the thrust pitching moment directly.

2. EXPERIMENTAL PROCEDURE

2.1 Test Equipment

The schematic diagram of the experimental facilities is shown in Fig.1. The inlet of the nozzle is exposed to the atmosphere, whereas a large vacuum tank connected to the outlet of the nozzle to achieve the pressure difference in nozzle. Pressurized dry air is used as the source for the secondary jet. The static pressure was measured using strain-type pressure gauges (PG-2KU and PG-20KU: Kyowa Electronic Instrument Co.) with the pressure probes. A standard Schlieren system was used to visualize the flow inside the nozzle. The NPL argon nano-pluse light is used as the light source [17].

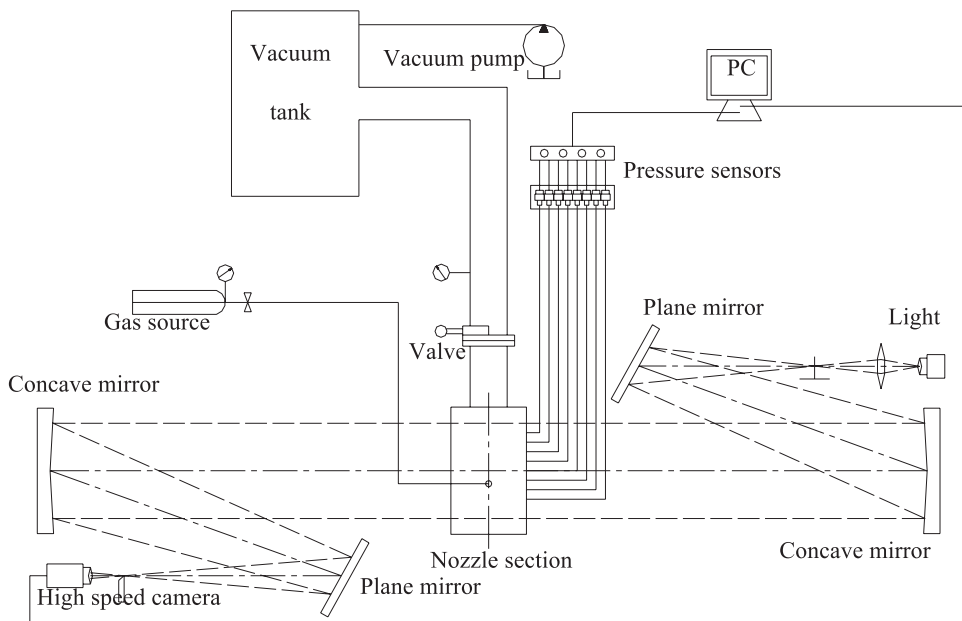


Figure 1. Schematic diagram of experimental setup.

2.2 Parameters in Experiment and Computation

Nozzle pressure ratio (NPR) is the ratio of main flow total pressure to the nozzle back pressure, whereas the secondary pressure ratio (SPR) is the ratio of the total pressure of secondary jet to the main flow total pressure. The distance (L_j) is the distance between the secondary jet injection slot and the nozzle exit. The conditions in experiments and numerical simulations range NPR from 3 to 10, SPR from 1 to 3, with $L_j = 0.005$ m and $L_j = 0.01$ m.

3. NUMERICAL STUDY

3.1 Numerical Scheme

The Reynolds number of the flow at the nozzle exit corresponds to the transition zone from laminar to turbulent flow. The flow at the inlet is smooth accelerated from the stationary atmosphere and the transition is expected to be suppressed till relatively high Reynolds number. This is visually confirmed

with Schlieren images. The Navier-Stokes equations together with mass, momentum and energy conservation equations are solved numerically [18]. The numerical fluxes are evaluated with the HLLC approximate Riemann solver for it can satisfy entropy property, and resolve isolated shock efficiently [19-20]. The numerical simulations were carried out with the WAF method. The WAF scheme is one of the higher order extensions of the Godunov scheme in both space and time [21].

3.2 Initial and Boundary Conditions

Initial and boundary conditions are defined to properly initialize and constrain the flow. The inflow boundary condition is fixed to the atmospheric conditions, the outflow boundary condition are calculated from the NPR, and the jet boundary condition is determined by the SPR. Computations were carried out for combinations of NPR, SPR and Lj corresponding to those in experiments.

4. EVALUATIONS OF FTV PERFORMANCE

The FTV performance is evaluated by thrust pitching angle δ_p [22-23].

$$\delta_p = \tan^{-1} \frac{F_N}{F_A}, \quad (1)$$

$$F_N = \sum (\rho uv) \cdot \Delta A, \quad (2)$$

$$F_A = \sum \{ \rho u^2 + (p - p_\infty) \} \cdot \Delta A, \quad (3)$$

where F_A and F_N are the x and y components of momentum, ρ and ΔA are density and cell area, u and v are the x and y components of velocity, and p and p_∞ are the static pressure and back pressure of cells at the x direction.

The thrust pitching moment M_p of the nozzle is calculated by integrating the product of the pressure on the nozzle walls and the length from a specific pivot point to the pressure working point, where l is the length from the working point to the pivot point and F_w is the working pressure [24].

$$M_p = \sum (F_w \cdot l) \quad (4)$$

5. RESULTS AND DISCUSSION

5.1 Nozzle model 1

5.1.1 Structure of nozzle

Figure 2 shows the structure of the FTV nozzle model 1.

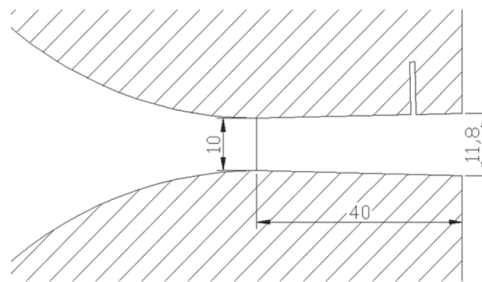


Figure 2. Structure of two-dimensional nozzle model 1.

The model is a rectangular cross-sectional nozzle with a throat area of 0.04m² and the expansion ratio (exit area divided by throat area) of 1.18. With this nozzle expansion ratio, the flow Mach number at the nozzle exit is calculated to be 1.5 according to an inviscid quasi-one-dimensional analysis. An independently-operated injection port on the upper of the nozzle diverging part has a width of 0.001 m.

5.1.2 Parameter distributions

Figure 3 shows flow Mach number distributions for SPR = 2 with NPR = 9 and Lj = 0.005 m or 0.01

m. The main flow accelerates in the converging section of the nozzle and reaches sonic speed at the throat and then becomes supersonic in the diverging section.

When L_j is small, it is observed that a wide region upstream of the secondary jet is disturbed as shown in Fig. 3(a) and the flow becomes subsonic in most of the nozzle diverging section. As L_j increases, as shown in Fig. 3(b), the distributed region is shifted toward upstream. The main flow is blocked by the secondary jet and the velocity of main flow becomes supersonic only for a small region near the throat.

Despite the strong influence of the secondary jet in the nozzle, the deflection of the exhaust gas is small and no relation with the value of L_j is found. We concluded that the effect of secondary jet to the main nozzle flow is too strong to study the FTV performance.

In this study, therefore, we decided to develop a new nozzle model 2 to avoid complex wave interactions in the nozzle diverging part.

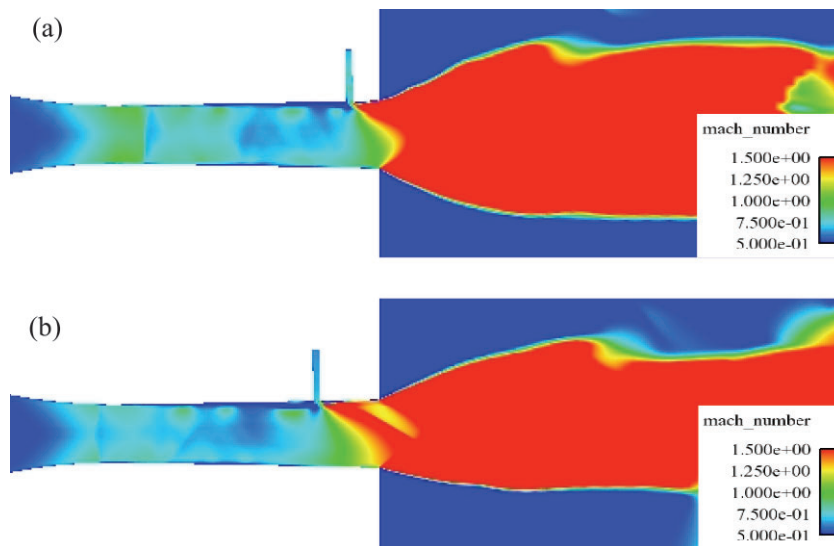


Figure 3. Mach number distribution with NPR = 9 and SPR = 2 and (a) $L_j = 0.005$ m or (b) $L_j = 0.01$ m

5.2 Nozzle model 2

5.2.1 Structure of nozzle

The nozzle model 2 is designed to rotate around the rotation shaft to adjust the exit spacing while keeping the throat spacing constant. The rotation shaft is set at 0.07 m from of the nozzle throat. The expected flow Mach numbers at the nozzle exit ranges from 1.44 to 2.55. In order to get the flow Mach number of 2, the area ratio of the nozzle exit to the throat area is 1.69. In order to observe the flow distribution in the nozzle in detail, the sizes of the nozzle throat and length of nozzle diverging part are designed to twice of nozzle model 1.

The secondary jet injection slot on the upper nozzle wall has a width of 0.001 m as same as nozzle model 1. Figure 4 shows the dimensions of nozzle with secondary jet injection slot adjusted to the flow Mach number of 2.

5.2.2 Flow around the secondary jet stream

Figure 5 shows the schematics of flow velocity configuration around the secondary jet slot with SPR = 1 and SPR = 2.

It shows the interaction of the secondary jet with the main nozzle flow. The secondary jet works as obstruction and the boundary layer is separated due to the adverse pressure gradient and a shock system is formed. The oblique shock wave generated in this manner will deflect the main flow downwards if the jet is injected from the upper wall. This is the mechanism that is normally expected for the FTV using oblique shock wave. As shown in Fig. 5(a), with a smaller value of SPR, the velocity of the flow upstream the secondary jet near the wall and domain of vortices are small. The secondary jet is turned back toward the nozzle wall and

re-attaches to the wall. As shown in Fig. 5(b), as the SPR increases, the vortices are strong and the range of vortices is larger and the separated area behind the secondary jet is connected to the region outside the nozzle exit.

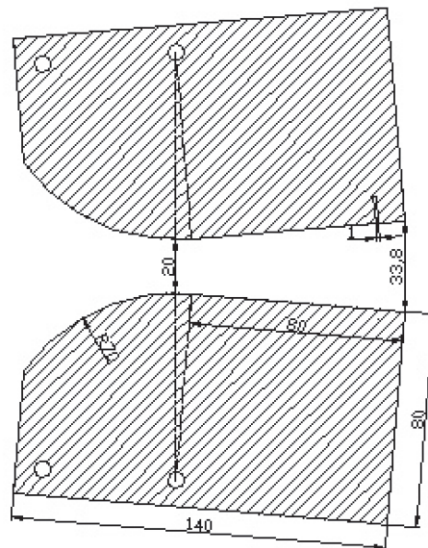


Figure 4. Dimensions of nozzle model 2 at Mach number of 2.

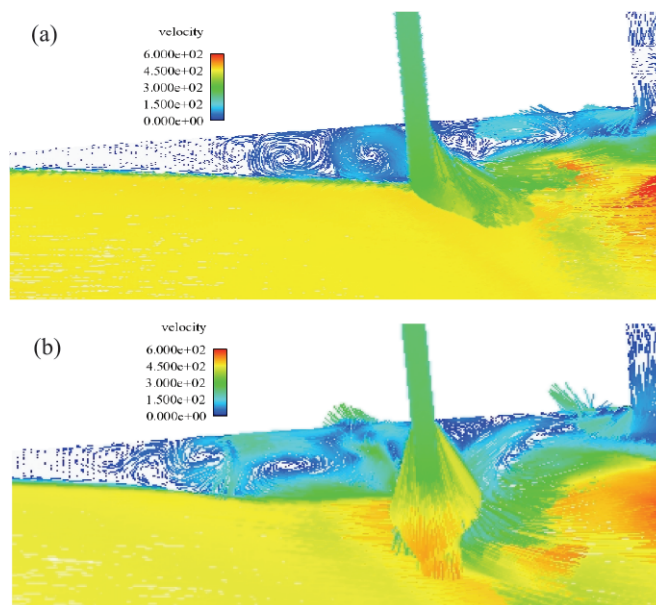


Figure 5. Velocity vector distribution near the secondary jet injection with NPR = 9 and (a) SPR = 1 or (b) SPR = 2.

5.2.3 Effect of NPR

In order to evaluate the effect of NPR, flows in the nozzle without secondary jet are investigated first. With the nozzle that is setup for the Mach number 2, the flows are over-expanded or under-expanded depending on if the value of NPR is below or above 7.8. Figure 6 shows the flow field with NPR = 3 and NPR = 9. The flow is over-expanded at NPR = 3 with oblique shock waves downstream of the nozzle exits. Whereas, the flow is under-expanded at NPR = 9 with oblique expansion waves outside the nozzle exit. Near the nozzle throat, two clear oblique shocks are visible. The waves are generated

at the throat where the secondary derivatives of the upper and lower nozzle surface geometry are discontinuous. In the upstream of the throat, wall surfaces are curved, while downstream of the point, the walls are straight.

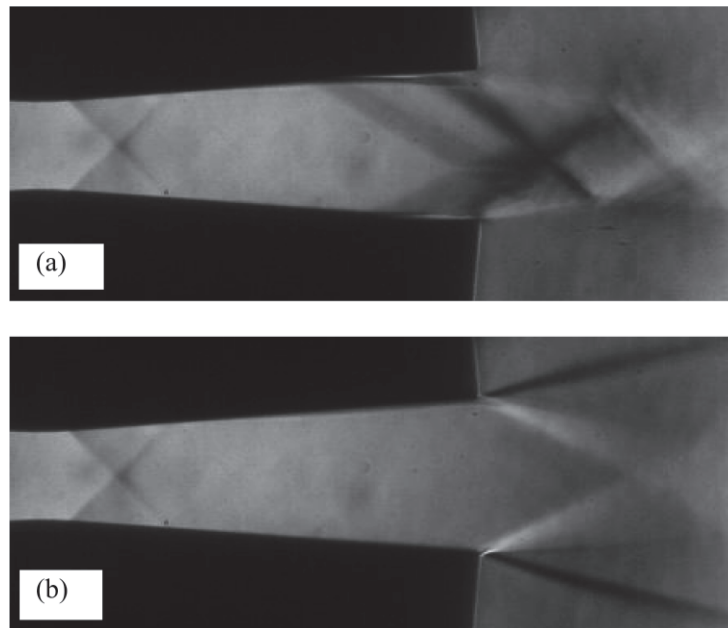


Figure 6. Schlieren images of different NPR and (a) NPR = 3 or (b) NPR = 9.

For the case of nozzle main flow with secondary jet injection, the thrust pitching moment and thrust pitching angle are used to evaluate the nozzle FTV performance. The pivot point for evaluating the pitching moment is chosen at the throat, and the counterclockwise moment is defined as positive and is expected to be positive if the main flow is deflected downward by an oblique shock wave. The pitching moment and pitching angle for different NPR ranging from 4 to 10 with $SPR = 1$, are shown in Table 1. It is found that most of the moments are positive as expected as the effect of the oblique shock wave FTV mechanism except at $NPR = 4$ for $L_j = 0.01$ m. The moments become larger with the NPR increases. The tendency of angle change is almost the same as that of moment. The inter-positive relation between angle and moment with $NPR = 4$ is unclear compared to the other larger NPR since the flow is unstable with the low NPR. For the case of $SPR = 2$, the inter-positive relation between the pitching moment and pitching angle is also found.

Table 1. M_p and δ_p with different NPR at $SPR = 1$ and $L_j = 0.005$ m and 0.01 m

NPR		4	5	6	7	8	9	10
$L_j = 0.005$ m,	δ_p [deg]	-1.378	.954	2.684	3.556	3.674	4.448	5.004
$L_j = 0.01$ m,	δ_p [deg]	1.532	1.774	2.826	2.598	3.028	4.178	4.426
$L_j = 0.005$ m,	M_p [N · m]	0.361	1.886	3.454	6.826	8.152	10.278	11.755
$L_j = 0.01$ m,	M_p [N · m]	-0.483	1.107	3.578	3.594	6.389	7.950	9.467

5.2.4 Effect of SPR

Figure 7 shows the density distributions for $L_j = 0.01$ m with $NPR = 9$ and $SPR = 1, 2$ and 3 . As shown in the figure, notable shock waves are observed at the upstream of the secondary jet slot and the shock waves are reflected at the jet boundary. The flow separation is also seen upstream of the secondary jet.

As shown in Fig. 7(a), in the case of $SPR = 1$, a weak shock wave far from the secondary jet and a strong shock wave upstream of the secondary jet are seen. As shown in Fig. 7(b), as SPR increases, the shock waves become stronger and, upstream the secondary jet, some weak shock waves also appear. As shown in Fig. 7(c), as SPR is increased further, the shock waves become stronger, and the domain of flow separation also becomes larger due to the strong secondary injection.

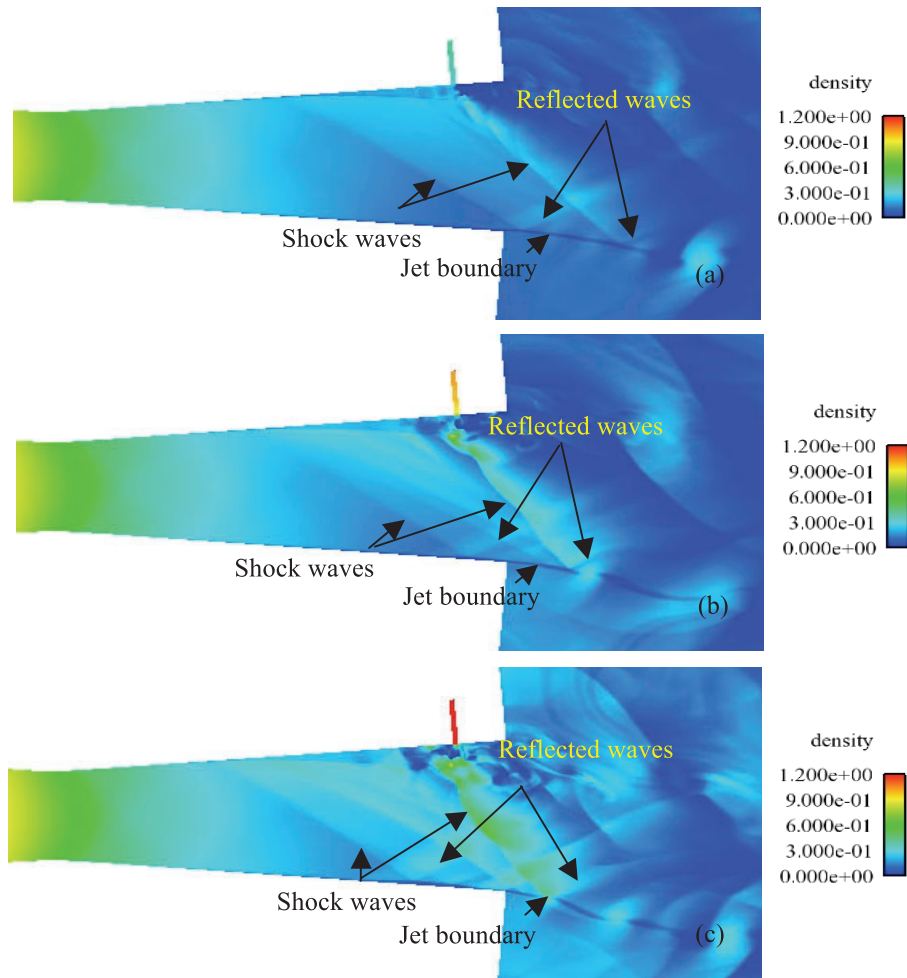


Figure 7. Density distribution in the nozzle diverging part with NPR = 9 and (a) SPR = 1 or (b) SPR = 2 or (c) SPR = 3.

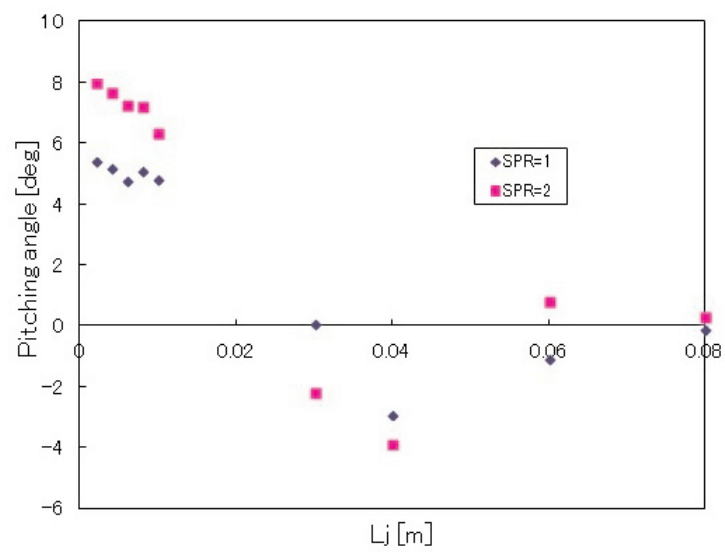


Figure 8. Thrust pitching angle at different L_j with NPR = 9.

5.2.5 Effect of L_j

The L_j increases with the secondary jet slot moving to the nozzle throat, L_j being the distance between the secondary jet slot and the nozzle exit. In order to investigate the effect of L_j quantitatively, Figure 8 shows the thrust pitching angle at different L_j with $NPR = 9$. It is observed the deflection angle decreases as the L_j increases to 0.01 m, that is to say, as the secondary jet slot is near the nozzle throat, the effect of the secondary jet on deflection angles becomes weak. Most of the angles are negative for the L_j from 0.02 m to 0.08 m due to wave reflections at the lower nozzle wall.

Fig. 9 shows the thrust pitching moment at different L_j with $NPR = 9$. It is observed that the moment decreases as the L_j increases to 0.01 m, that is to say, as the secondary jet slot moves to the nozzle throat, the effect of the secondary jet on pitching moment becomes weaker. It is also found that the negative moments are caused by the wave reflections at the lower nozzle wall. The tendency of Fig. 9 is the same as the pitching angle in Fig.8. This is also said that larger moment generates the larger deflection angle.

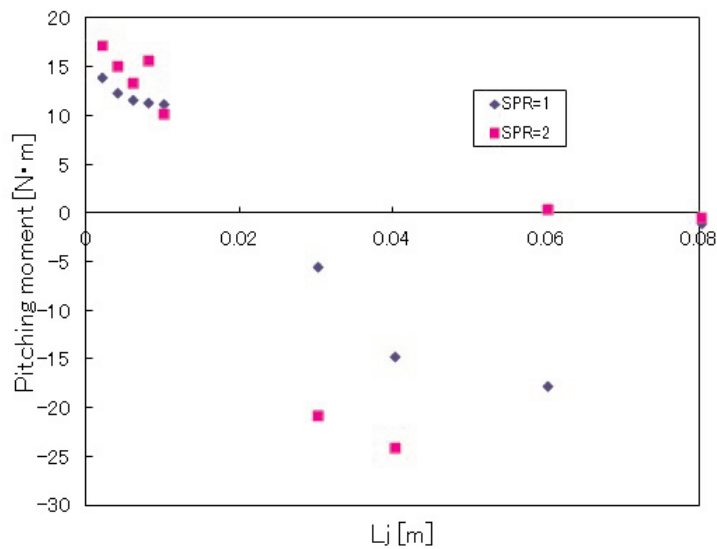


Figure 9. Thrust pitching moment at different L_j with $NPR = 9$.

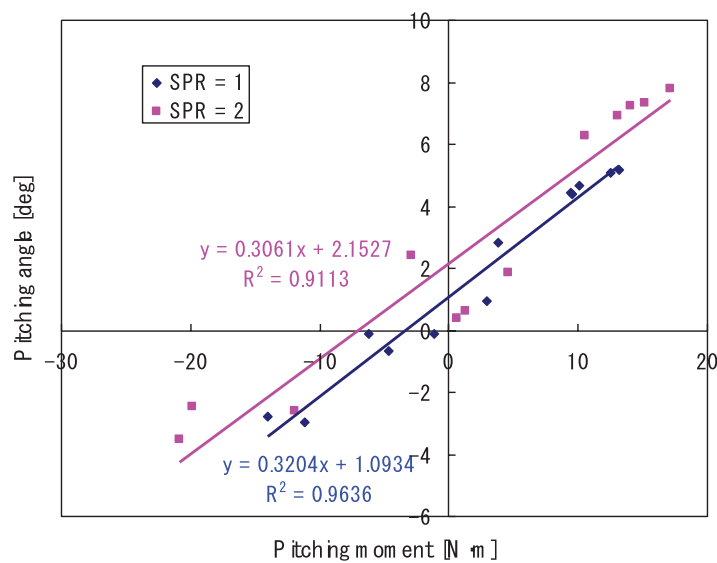


Figure 10. Relation between thrust pitching moment and thrust pitching angle.

In this study, two methods using the force-moment and the pitching angle have been used to evaluate the FTV performance. The relation between the thrust pitching moment and thrust pitching angle is shown in Fig.10. The regression equation and coefficient of determination of $SPR = 2$ is gotten by the same way. The regression equations show that the larger the moment is, the larger is the deflection angle. The coefficients of determination of two cases are high above 0.9.

6. CONCLUSIONS

The interaction of a secondary jet with the primary jet flow, and the effect of FTV parameters on FTV performance in two nozzle models have been investigated. The experiments and numerical simulations are carried out and are performed with and without the secondary jet injection for different combinations of NPR, SPR, and jet location. The effects of FTV parameters, such as the NPR, SPR and L_j have direct effects on the performance.

The performance of FTV is evaluated by thrust pitching moment and thrust pitching angle. The relation between the thrust pitching moment and the thrust pitching angle shows the positive inter-relation between them. Therefore, FTV performance can be evaluated with the thrust pitching moment directly.

ACKNOWLEDGMENTS

This work was sponsored by the Scientific Research Foundation for the Returned Overseas Chinese Scholars, State Education Ministry. This study was also supported by the cooperative research program of the Earthquake Research Institute, the University of Tokyo, Japan.

REFERENCES

- [1] K. A. Deere, Computational Investigation of the Aerodynamic Effects on Fluidic Thrust Vectoring, *36th AIAA/ASME/SAE/ASEE Joint Propulsion Conference & Exhibit July 17-19, 2000* / Huntsville, AL, 2000.
- [2] P. C. Murphy and J. B. Davidson, Control Design for Future Agile Fighters. *AIAA Paper No. 91-2882*. Atmospheric Flight Mechanics Conference, New Orleans, Louisiana. 1991.
- [3] J. S. Orme, Ross Hathaway, *Initial Flight Test Evaluation of the F-15 ACTIVE Axisymmetric Vectoring Nozzle Performance*, NASA/TM-1998-206558.
- [4] S. C. Asbury, *Internal Performance of a Fixed-Shroud Nonaxisymmetric Nozzle Equipped with an Aft-Hood Exhaust Deflector*, NASA/TM-97-206255, 1997.
- [5] A. J. Neely, F. N. Gesto and J. Young, Performance Studies of Shock Vector Control Fluidic Thrust Vectoring, *AIAA-2007-5086*, *43rd AIAA/ASME/SAE/ASEE Joint Propulsion Conference & Exhibit*, Cincinnati, OH, 2007.
- [6] K. A. Deere, *Summary of Fluidic Thrust Vectoring Research Conducted at NASA Langley Research Center*, AIAA-2003-3800.
- [7] J. G. Taylor, *A Static Investigation of a Simultaneous Pitch and Yaw Thrust Vectoring 2-D C-D Nozzle*, AIAA 88-2998.
- [8] J. D. Flamm, K.A. Deere, Design Enhancements of the Two-Dimensional, Dual Throat Fluidic Thrust Vectoring Nozzle Concept, *AIAA 2006-3701*, *3rd AIAA Flow Control Conference*, San Francisco, California, 2006.
- [9] E. Gamble and D. Haid, *Improving Off-design Nozzle Performance Using Fluidic Injection*. AIAA-2004-1206, 2004.
- [10] R. J. Shyne, *A Survey of Challenges in Aerodynamic Exhaust Nozzle Technology for Aerospace Propulsion Applications*, NASA/TM-2002-211977.
- [11] A. J. Neely, Fernando N. Gesto, Performance Studies of Fluidic Vector Control Fluidic Thrust Vectoring, *43rd AIAA/ASME/SAE/ASEE Joint Propulsion Conference & Exhibit*, Cincinnati, OH, AIAA-2007-5086.
- [12] M. S. Mason, William J. Crowther, Fluidic Thrust Vectoring of Low Observable Aircraft, *CEAS Aerospace Aerodynamic Research Conference*. 2002.
- [13] E. G. Collins, Feedback Control for Counterflow Thrust Vectoring, *Proceeding of the 2004 American Control Conference*, Boston, Massachusetts. 2004.

- [14] P. J. Yagle, D. N. Miller, Demonstration of Fluidic Throat Skewing for Thrust Vectoring in Structurally Fixed Nozzles, *ASME Journal of Engineering for Gas Turbines and Power*, 2001.
- [15] K. A. Waithe, Karen A. Deere, Experimental and Computational Investigation of Multiple Injection Ports in a Convergent-Divergent Nozzle for Fluidic Thrust Vectoring, *21st AIAA Applied Aerodynamics Conference AIAA-2003-3802*.
- [16] E. Gamble, D. Haid, *Improving Off-Design Nozzle Performance Using Fluidic Injection*, AIAA-2004-1206.
- [17] L. Li, M. Hirota, and T. Saito, Numerical and Experimental Studies of Fluidic Thrust Vectoring, *28th International Symposium on Shock Waves*, UK. 2011.
- [18] E. F. Toro, *Riemann Solvers and Numerical Methods for Fluid dynamics (2nd Edition)*, Springer-Verlag Berlin Heidelberg. 1999.
- [19] James J. Quirk, *A Contribution to the Great Riemann Solver Debate*, NASA Contractor Report 191409 ICASE Report No. 92-64, 1992.
- [20] Sung Don Kim, Bok Jik Lee, Robust HLLC Riemann Solver with Weighted Average Flux Scheme for Strong Shock, *Journal of Computational Physics*, 2009.
- [21] S. J. Billett and E. F. Toro, On WAF-Type Schemes for Multidimensional Hyperbolic conservation Laws, *Journal of Computational Physics* 130, pp: 1-24. 1997.
- [22] Mark S. Mason, William J. Crowther, Fluidic Thrust Vectoring of Low Observable Aircraft, *CEAS Aerospace Aerodynamic Research Conference*, 2002.
- [23] David J. Wing, Victor J. Giuliano, Fluidic Thrust Vectoring of an Axisymmetric Exhaust Nozzle at Static Conditions, *ASME Fluids Engineering Division Summer Meeting*, 1997.
- [24] Li Li, Tsutomu Saito, Numerical and Experimental Investigations of Fluidic Thrust Vectoring Mechanism, *International Journal of Aerospace Innovations*, 4(1-2), pp: 53-64, 2012.